Modelling Reflections via Multiperspective Imaging

Jingyi Yu
Massachusetts Institute of Technology
Cambridge, MA 02139
jingyi@graphics.lcs.mit.edu

Leonard McMillan
University of North Carolina
Chapel Hill, NC 27599
mcmillan@cs.unc.edu

Abstract

We present a novel method for analyzing reflections on arbitrary surfaces. We model reflections using a broader than usual class of imaging models, which include both perspective and multiperspective camera types. We provide an analytical framework to locally model reflections as specific multiperspective cameras around every ray based on a new theory of general linear cameras. Our framework better characterizes the complicated image distortions seen on irregular mirror surfaces as well as the conventional catadioptric mirrors. We show the connection between multiperspective camera models and caustic surfaces of reflections and demonstrate how they reveal important surface rulings of the caustics. Finally, we show how to use our analysis to assist mirror design and characterize distortions seen in catadioptric imaging systems.

1. Introduction

Reflections are important visual phenomena, as well as a potential class of images suitable for analysis by computer vision. Although the basic physics and the geometry of reflections are well understood, analyzing reflections on arbitrary mirror surfaces is still complicated, and quantitative classification of reflection distortions still remains an open problem. Most research on analyzing reflections has focused on catadioptric mirrors, such as hyperbolic and parabolic mirrors [17, 1, 12, 6, 19], to obtain single viewpoint (pinhole) optics. Different methods have been proposed to calibrate these catadioptric imaging systems [9, 17]. However, when the reflected rays do not converge to a single viewpoint, the corresponding imaging geometry becomes difficult to analyze [18].

In this paper, we propose a different method to analyze reflected images seen on arbitrary mirrors. While most previous research has been restricted to simple parametric reflectors such as spherical or conical mirrors [6, 19], and equiangular mirrors [15], our method applies to reflections off of any parametric or mesh surface. Our goal is to model the group behavior of each reflected ray and its neighboring rays as if they are captured from a multiperspective camera. Our approach is to first map reflections to two-dimensional manifolds in a four-dimensional ray space. At each point/ray on these reflection manifolds, the local tangent planes can be characterized to determine the local geometric properties of the reflection.

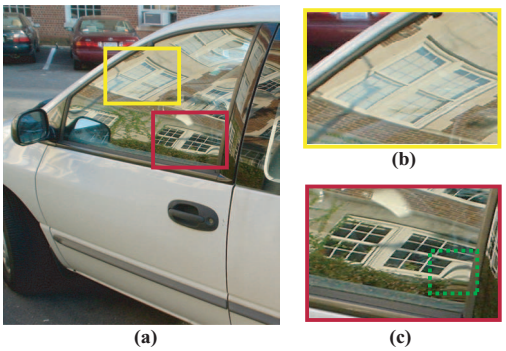

Figure 1. A reflected image seen on a car window. Subregions illustrate multiperspective distortions such as shearing (yellow), uneven aspect ratio (red), and duplications (green).

Our analysis is based on the recently proposed general linear camera (GLC) model [20] that characterizes all 2D planes in the ray space as one of the eight multiperspective cameras. This analysis allows us to identify the type of the GLC camera at each point in a reflected image. Our framework shows that, when viewed from a pinhole or an orthographic camera, local reflections seen on mirror surfaces can originate from only four of the eight possible GLC cameras – pushbroom [8], cross-slit [22], pinhole, or orthographic cameras. The imaging properties of these multiperspective GLCs explain the distortions seen in a reflected image. We show how these distortions relate to their local GLC type, and how the GLC type dictates reflection properties. Furthermore, we show the caustic surface relates to the geometric features of cross-slit cameras. In general, the

Proceedings of the 2005 IEEE Computer Society Conference on Computer Vision and Pattern Recognition (CVPR'05)
1063-6919/05 $20.00 © 2005 **IEEE**

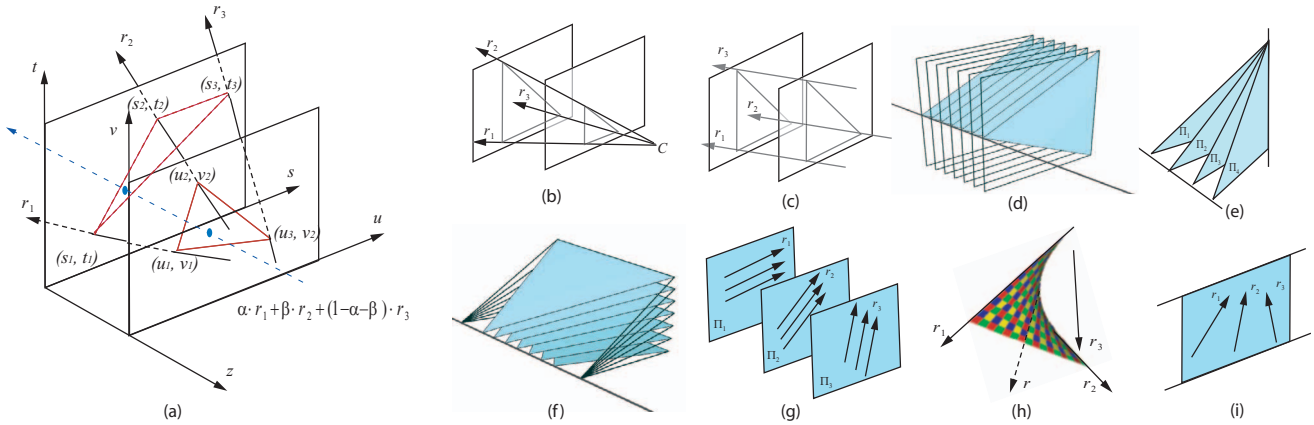

Figure 2. General Linear Camera Models. (a) A GLC Model collects radiance along all possible affine combination of three rays. The rays are parameterized by their intersections with two parallel planes. There are precisely eight GLCs, shown in (b) to (i). (b) In a pinhole camera, all rays pass through a single point. (c) In an orthographic camera, all rays are parallel. (d) In a pushbroom, all rays lie on a set of parallel planes and pass through a line. (e) In a cross slit camera, all rays pass through two non-coplanar lines. (f) In a pencil camera, all coplanar rays originate from a point on a line and lie on a specific plane through the line. (g) In a twisted orthographic camera, all rays lie on parallel twisted planes and no rays intersect. (h) In an bilinear camera, no two rays are coplanar and no two rays intersect. (i) In an EPI camera, all rays lie on a 2D plane.

two slits rule the caustic surface and determine the orientation of the distortions as well as the aspect ratio seen in the reflected image.

Our method works for either parametric or mesh surfaces. We show how to locally model reflected rays as GLCs in both cases. Our method works robustly with coarse mesh surfaces and accurately predicates reflection distortions. Finally, we show how to use our framework to assist mirror design and to improve catadioptric imaging systems.

Before proceeding, we explain our notation. Superscripts, such as p^x, p^y, and p^z represent the x and y and z coordinate of a point or vector. Subscripts, such as f_x and f_y represents the first-order partial derivatives of f with respect to x and y. And similarly, f_{xx} refers to the second-order partial derivative of f with respect to x.

2. Previous Work

The classic pinhole camera model collects rays passing through a single point. Because of its simplicity, this single viewpoint camera model is commonly used to analyze reflections. Catadioptric imaging systems place a virtual pinhole camera at the focus of a hyperbolic or parabolic surface to synthesize a pinhole camera with a wider field of view [12, 1]. This setup requires accurate alignment of the viewing camera [9, 17]. When the camera moves off the focus, the caustic surface of the rays quickly evolves into complicated shapes with discontinuities such as cusps [17, 18]. Closed-form solutions of caustics are restricted to mirrors with simple shapes [17, 15]. The caustic surface models every ray as originating from a single, but spatially varying, pinhole, and it does not provide much insight into the group behavior of neighboring rays, and hence, cannot be used for interpreting the imaging properties at local regions of the reflected image.

Alternative camera representations known as multiperspective cameras, capture rays from spatially varying viewpoints. Multiperspective cameras include pushbroom cameras [8], which collect rays along parallel planes from points swept along a linear trajectory, and Cross-slit cameras, which collect all rays passing through two lines. Zomet et al [22] did an extensive analysis and modelling of Cross-slit (XSlit) multiperspective cameras. Swaminathan and Nayar [16] also analyzed the distortion of multiperspective images with known scene geometry.

2.1. General Linear Cameras

Yu and McMillan [20] proposed a general linear camera (GLC) model that unifies traditional perspective, orthographic, and multiperspective cameras models. In the GLC framework every ray is parameterized by its intersections with the two parallel planes, where $[s, t]$ is the intersection with the first and $[u, v]$ the second, as shown in Figure 2a. This parametrization is often called a two-plane parametrization (2PP) [11, 7]. Except for rays parallel to the two planes, 2PP uniquely represents each ray by mapping it to a point in a 4D ray space.

A GLC is defined as the affine combination of three rays:

$$GLC = \{r : r = \alpha \cdot [s_1, t_1, u_1, v_1] + \beta \cdot [s_2, t_2, u_2, v_2] + (1 - \alpha - \beta) \cdot [s_3, t_3, u_3, v_3], \forall \alpha, \beta\}$$

Many well-known multiperspective cameras, such as push-broom, cross-slit, linear oblique cameras are GLCs. Furthermore, [20] provides a characteristic equation to determine the type of the multiperspective camera for any GLC specification:

$$\begin{vmatrix} \lambda \cdot s_1 + (1-\lambda) \cdot u_1 & \lambda \cdot t_1 + (1-\lambda) \cdot v_1 & 1 \\ \lambda \cdot s_2 + (1-\lambda) \cdot u_2 & \lambda \cdot t_2 + (1-\lambda) \cdot v_2 & 1 \\ \lambda \cdot s_3 + (1-\lambda) \cdot u_3 & \lambda \cdot t_3 + (1-\lambda) \cdot v_3 & 1 \end{vmatrix} = 0 \tag{1}$$

The number of solutions to this quadratic equation in λ determines how many singularities (lines or points) that all rays in the GLC can pass through. A total of eight GLC types describe all 2D linear manifolds in the ray space, and their imaging geometries are shown in Figure 2.

We simplify the analysis of [20] by substituting $\sigma = s - u$ and $\tau = t - v$. In this paper, we use this $[\sigma, \tau, u, v]$ parametrization to represent rays. We also assume the default uv plane is at $z = 0$ and st plane at $z = 1$. With this new parametrization, the characteristic equation (1) simplifies to

$$\begin{vmatrix} u_1 + \lambda \cdot \sigma_1 & v_1 + \lambda \cdot \tau_1 & 1 \\ u_2 + \lambda \cdot \sigma_2 & v_2 + \lambda \cdot \tau_2 & 1 \\ u_3 + \lambda \cdot \sigma_3 & v_3 + \lambda \cdot \tau_3 & 1 \end{vmatrix} = 0 \tag{2}$$

resulting in a quadratic equation $A\lambda^2 + B\lambda + C = 0$ where

$$\begin{aligned} A &= \begin{vmatrix} \sigma_1 & \tau_1 & 1 \\ \sigma_2 & \tau_2 & 1 \\ \sigma_3 & \tau_3 & 1 \end{vmatrix}, \quad C = \begin{vmatrix} u_1 & v_1 & 1 \\ u_2 & v_2 & 1 \\ u_3 & v_3 & 1 \end{vmatrix} \\ B &= \begin{vmatrix} \sigma_1 & v_1 & 1 \\ \sigma_2 & v_2 & 1 \\ \sigma_3 & v_3 & 1 \end{vmatrix} - \begin{vmatrix} \tau_1 & u_1 & 1 \\ \tau_2 & u_2 & 1 \\ \tau_3 & u_3 & 1 \end{vmatrix} \end{aligned} \tag{3}$$

Given any GLC, one can determine its type examining its A coefficient and discriminant $\Delta = B^2 - 4AC$ of its characteristic equation.

3. Reflection Ray Manifold

Reflected images can be analyzed using the GLC framework. Given a viewing camera and a mirror surface, we can map each reflected ray into $[\sigma, \tau, u, v]$ ray space. Assume the mirror surface is of form $z(x, y)$. We can compute every reflected ray as follows:

$$\vec{r} = \vec{i} - 2(\hat{n} \cdot \vec{i})\hat{n} \tag{4}$$

where $\vec{i}$ is the incident ray and $\hat{n}$ is a unit normal that can be computed by normalizing $[-z_x, -z_y, 1]$. Intersecting the ray with the st and uv plane as shown in Figure 3, the $[\sigma, \tau, u, v]$ coordinate of the ray can be computed as:

$$[\sigma, \tau, u, v] = [\frac{r^x}{r^z}, \frac{r^y}{r^z}, x - z \cdot \frac{r^x}{r^z}, y - z \cdot \frac{r^y}{r^z}] \tag{5}$$

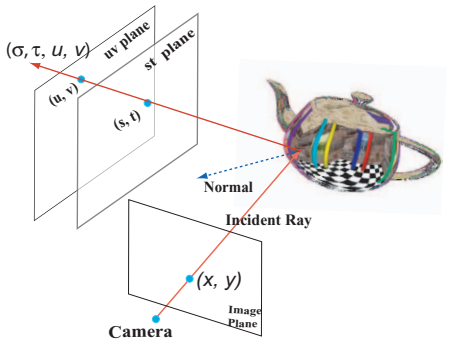

Figure 3. At each point on the surface, the reflected ray is mapped into the ray space by intersecting with the two parametrization planes.

All variables r, z, σ, τ, u, and v are functions in x and y, hence, the set of reflection rays from the mirror surface form a ray-space parametric manifold in x and y

$$\Sigma(x, y) = [\sigma(x, y), \tau(x, y), u(x, y), v(x, y)] \tag{6}$$

At every (x, y), we can compute the local tangent plane in 4D. The tangent plane describes the local behavior of the reflections. Recall that all planes in the ray space are characterized by one of the eight types of GLCs, thus, the local tangent plane reveals the unique multiperspective properties around every reflection ray.

At every point on the reflected image manifold $[\sigma, \tau, u, v]$, a tangent plane can be computed with two spanning vectors $\vec{d_1}$ and $\vec{d_2}$:

$$\vec{d_1} = [\sigma_x, \tau_x, u_x, v_x], \vec{d_2} = [\sigma_y, \tau_y, u_y, v_y] \tag{7}$$

Its characteristic equation can be computed by choosing three points on the tangent plane, which are $\Sigma(x, y)$, $\Sigma(x, y) + \vec{d_1}$, and $\Sigma(x, y) + \vec{d_2}$ using (2) as:

$$\begin{vmatrix} u + \lambda\sigma & v + \lambda\tau & 1 \\ (u + u_x) + \lambda(\sigma + \sigma_x) & (v + v_x) + \lambda(\tau + \tau_x) & 1 \\ (u + u_y) + \lambda(\sigma + \sigma_y) & (v + v_y) + \lambda(\tau + \tau_y) & 1 \end{vmatrix} = 0 \tag{8}$$

yielding to the quadratic equation $A\lambda^2 + B\lambda + C = 0$ where

$$\begin{aligned} A &= \sigma_x\tau_y - \sigma_y\tau_x \\ B &= \sigma_x v_y - \sigma_y v_x - \tau_x u_y + \tau_y u_x \\ C &= u_x v_y - u_y v_x \end{aligned} \tag{9}$$

The discriminant, Δ, can be computed as

$$\begin{aligned} \Delta &= (\tau_y u_x - \tau_x u_y + \sigma_x v_y - \sigma_y v_x)^2 \\ &- 4(\sigma_x\tau_y - \sigma_y\tau_x)(u_x v_y - u_y v_x) \end{aligned} \tag{10}$$

The edge-parallel condition [20], used to distinguish pinholes from pencils, and twisted orthographic from ortho-

Table 1. Characterize General Linear Cameras by Characteristic Equation

Characteristic Equation	2 Solution	1 Solution	0 Solution	∞ Solution
$A \neq 0$	XSlit	Pencil/Pinhole†	Bilinear	Ø
$A = 0$	Ø	Pushbroom	Twisted/Ortho.†	EPI

†: A GLC satisfying *edge-parallel* condition is pinhole($A \neq 0$) or orthographic ($A = 0$).

graphic cameras, is given as

$$\begin{aligned} &\sigma_x v_x - \tau_x u_x = 0, \quad \sigma_y v_y - \tau_y u_y = 0 \\ &(\sigma_x - \sigma_y)(v_x - v_y) - (\tau_x - \tau_y)(u_x - u_y) = 0 \end{aligned} \tag{11}$$

4. Differential Invariant Property

The GLC camera type is determined by, A, Δ, and the edge-parallel equation under the default parametrization planes, as shown in Table 1. Next we address what happens when we choose a different set of parametrization planes. Apparently, the same rays will have different ray coordinates under the new parametrization and the reflection ray manifold will be different from the original one. The local tangent plane at the same ray will also be different under the new parametrization. An intrinsic reflection property would reveal that the behavior of rays is independent of their parametrization, i.e., local reflections around the same ray should correspond to the same multiperspective camera model under different parametrization planes. We show the GLC analysis satisfies this invariant property. Specifically, we show that the signs and zeros of the characteristic equation's A and Δ terms, as well as the edge-parallel condition, are invariant to the parametrization.

Given a set of rays that map to a 2D manifold under the default parametrization, we first compute the transformation from the old manifold to the new one. Assume the new parametrization planes are specified by two points $\dot{p}$ and $\dot{q}$ on each of the planes, and two spanning directions $\vec{d_1}$, $\vec{d_2}$ of the plane. For every ray $[\sigma, \tau, u, v]$ on the old manifold, we compute intersections of the ray with the two new planes $[s', t']$ and $[u', v']$ by solving the equations:

$$\begin{aligned} [u, v, 0] + \lambda_1[\sigma, \tau, 1] &= \dot{p} + \vec{d_1}s' + \vec{d_2}t' \\ [u, v, 0] + \lambda_2[\sigma, \tau, 1] &= \dot{q} + \vec{d_1}u' + \vec{d_2}v' \end{aligned} \tag{12}$$

It was shown in [20] that the characteristic equation of a GLC does not change when translated in the parametrization plane. Assuming the two planes are not parallel to the z axis, we can choose $\dot{p} = [0, 0, p^z]$ and $\dot{q} = [0, 0, q^z]$ to simplify our analysis. Otherwise, we can choose their intersections with with the x or y axis and similar results hold. The new $[\sigma', \tau', u', v']$ can be computed as:

$$\begin{aligned} \sigma' &= s' - u' = \frac{(p^z - q^z)(d_2^y\sigma - d_2^x\tau)}{\gamma} \\ \tau' &= t' - v' = \frac{(q^z - p^z)(d_1^y\sigma - d_1^x\tau)}{\gamma} \\ u' &= \frac{q^z(d_2^y\sigma - d_2^x\tau) + d_2^y u - d_2^x v + d_2^z(\sigma v - \tau u)}{\gamma} \\ v' &= \frac{q^z(d_1^x\tau - d_1^y\sigma) + d_1^x v - d_1^y u - d_1^z(\sigma v - \tau u)}{\gamma} \end{aligned}$$

where

$$\gamma = \begin{vmatrix} d_1^x & d_1^y & d_1^z \\ d_2^x & d_2^y & d_2^z \\ \sigma & \tau & 1 \end{vmatrix} \tag{13}$$

The new $[\sigma', \tau', u', v']$ parametrization is bilinear rational function of $\sigma,\ \tau,\ u,\ v$. The transformation has a singularity where γ is zero. This happens when the reflected ray is parallel to the new parametrization plane.

The spanning vectors of a tangent plane under the new parametrization can be computed by taking the partial derivations of $[\sigma', \tau', u', v']$ as $[\sigma'_x, \tau'_x, u'_x, v'_x]$ and $[\sigma'_y, \tau'_y, u'_y, v'_y]$ using the chain rule. The new characteristic equation can be computed using Equation (8).

As a result, the relationship between the default characteristic coefficients A and Δ as in (9) and (10) and the new ones A' and Δ' satisfy:

$$\begin{aligned} A' &= \frac{(d_1^x d_2^y - d_2^x d_1^y)^2 (p^z - q^z)^2 A}{\gamma^3} \\ \Delta' &= \frac{(d_1^x d_2^y - d_2^x d_1^y)^2 (p^z - q^z)^2 \Delta}{\gamma^4} \end{aligned} \tag{14}$$

The edge-parallel equations can be computed as:

$$\begin{aligned} &\sigma'_x v'_x - \tau'_x u'_x = \mu(\sigma_x v_x - \tau_x u_x) \\ &\sigma'_y v'_y - \tau'_y u'_y = \mu(\sigma_y v_y - \tau_y u_y) \\ &(\sigma'_x - \sigma'_y)(v'_x - v'_y) - (\tau'_x - \tau'_y)(u'_x - u'_y) \\ &= \mu((\sigma_x - \sigma_y)(v_x - v_y) - (\tau_x - \tau_y)(u_x - u_y)) \end{aligned}$$

where

$$\mu = \frac{(d_1^x d_2^y - d_2^x d_1^y)(p^z - q^z)}{\gamma^2} \tag{15}$$

Since the two planes intersect the z axis at two different points $\dot{p}$ and $\dot{q}$, $p^z - q^z \neq 0$. The two spanning vectors on the parametrization plane have to be different, so $d_1^x d_2^y - d_2^x d_1^y \neq 0$. Thus, $A' = 0$ if and only if $A = 0$. Similarly, the sign of Δ' is the same as Δ, and the new edge parallel condition is satisfied if and only if the original one is satisfied.

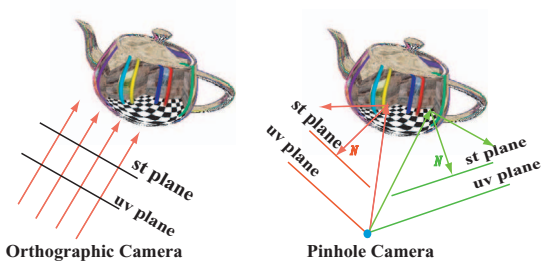

Figure 4. (a) If viewed from an orthographic camera, the parametrization plane is perpendicular to the incident direction. (b) If viewed from a pinhole camera, the parametrization plane at each point on the surface is parallel to its tangent plane.

5. Multiperspective Reflection Model

The differential invariant property provides the freedom to reparameterize any tangent plane to analyze the local GLC-type-specific behavior on the reflection manifold. In this section, we analyze reflections off of arbitrary mirror surfaces when viewed from orthographic and pinhole cameras.

5.1. Orthographic Viewing Camera

Orthographic cameras collect rays with a common direction. We choose the two parametrization planes perpendicular to the viewing directions so that all incident rays have direction $(0, 0, 1)$, as is shown in Figure 4. Assume the mirror surface is $z(x, y)$ with respect to the uv plane, at every point on the mirror, the $[\sigma, \tau, u, v]$ coordinate of the reflection ray can be computed using equation (4) as:

$$[\sigma, \tau, u, v] = [\frac{2z_x}{\alpha}, \frac{2z_y}{\alpha}, x - \frac{2z_x z}{\alpha}, y - \frac{2z_y z}{\alpha}] \qquad (16)$$

where

$$\alpha = z_x^2 + z_y^2 - 1 \qquad (17)$$

Notice, the denominator α is zero if and only if the reflected ray is parallel to the parametrization planes. If it happens, we can choose a different set of parametrization planes.

The resulting characteristic coefficients and edge-parallel equations are:

$$A = -K\frac{4\beta^3}{\alpha^3}, \quad B = -2zA - \frac{2\beta}{\alpha^2}(z_{xx} + z_{yy})$$
$$\Delta = \frac{4\beta^2}{\alpha^4}((z_{xx} - z_{yy})^2 + 4z_{xy}^4)$$
$$\sigma_x v_x - \tau_x u_x = \frac{2\beta}{\alpha^2} z_{xy}$$
$$\sigma_y v_y - \tau_y u_y = -\frac{2\beta}{\alpha^2} z_{xy}$$

$$(\sigma_x - \sigma_y)(v_x - v_y) - (\tau_x - \tau_y)(u_x - u_y) = \frac{2\beta}{\alpha^2}(z_{xx} - z_{yy}) \qquad (18)$$

where

$$\beta = z_x^2 + z_y^2 + 1$$
$$K = \frac{z_{xx} z_{yy} - z_{xy}^2}{(z_x^2 + z_y^2 + 1)^2} \qquad (19)$$

According to Table 1, if the local tangent plane has $A = 0$, the corresponding GLC is either a pushbroom camera when $B \neq 0$, or an orthographic/twisted orthographic cameras when $B = 0$. From equation (18), $A = 0$ if and only if $K = 0$. K represents the Gaussian curvature at the point. K is zero when the ray is reflected at parabolic points and planar points.

When $A = 0$ and $B = 0$, the local reflected GLC corresponds to an orthographic camera. We must have

$$z_{xx} = z_{xy} = z_{yy} = 0 \qquad (20)$$

This occurs when the local surface is flat, i.e., it is locally a planar mirror. It is also easy to verify that the edge-parallel equations are zero when $z_{xx} = z_{xy} = z_{yy} = 0$. Thus, local reflected rays cannot be a twisted orthographic camera. In the generic case when $A = 0$, the reflected rays at the parabolic points locally behave as a pushbroom camera. Koenderink [10] shows that specular reflections exhibit "duplications" at the parabolic points. This "duplication" is in fact a common feature for pushbroom cameras.

Now let us consider Δ and $A \neq 0$. From equation (18), $\Delta \geq 0$, i.e., the reflection tangent-plane GLCs cannot be of the bilinear GLC-type. Therefore, local reflected rays either behave like a cross-slit camera when $\Delta > 0$ or a pinhole/pencil when $\Delta = 0$. By equation (18), $\Delta = 0$ occurs only when

$$z_{xy} = 0 \quad and \quad z_{xx} = z_{yy} \qquad (21)$$

It is easy to verify that the edge-parallel equations in (18) are zero whenever $z_{xy} = 0$ and $z_{xx} = z_{yy}$. Therefore, all solutions with $\Delta = 0$ can only corresponds to pinhole GLC camera types. Solving equation (21) gives a paraboloid. A similar result has been shown in [1].

In general, local reflection images observed via an orthographic camera can only be cross-slit, pushbroom, pinhole, or orthographic images. No bilinear (oblique), twisted orthographic, or pencil images can be ever observed as a single-surface reflection image seen by an orthographic camera.

5.2 Pinhole Camera as View Camera

The analysis of a reflected image seen by a pinhole camera is more complicated. Assume that camera's center-of-projection is at the origin, the GLC differential invariant

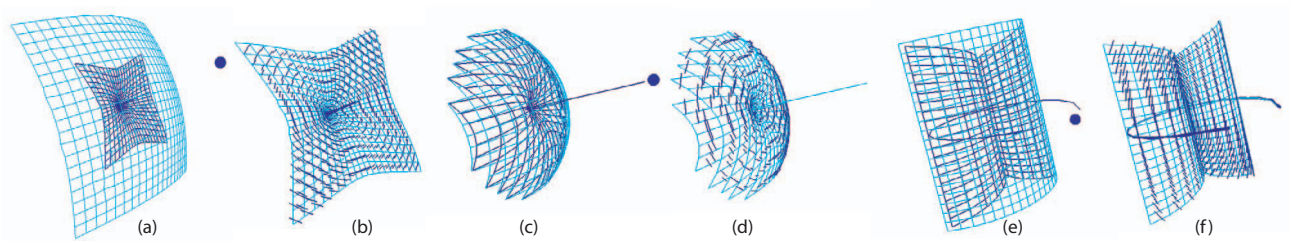

Figure 5. The caustic surface and its ruling of typical mirrors. The viewpoint is shown as a blue sphere. (a) A hyperbolic mirror. (c) A parabolic mirror. (e) A cylindrical mirror. (b), (d), and (f) show the ruling of the caustics of (a), (c), (e), respectively.

property allows us to choose a different parametrization for every reflected ray. We choose the parametrization planes parallel to the tangent plane of the 3D reflection surface at each reflected ray, and uv plane to pass through the origin, as shown in Figure 4. This transformation is analogous to the Legendre transformation of the curve equation [2, 13]. The mirror surface is also modelled as a Monge function $z(x, y)$ with respect to the parametrization planes. Under this choice of parametrization, we must have $z_x = z_y = 0$ at the reflected ray we analyze.

The direction (σ, τ) of the reflection ray can be computed using (4) as

$$\begin{aligned} \sigma &= \frac{x(z_x^2 - z_y^2 - 1) + 2z_x z_y y - 2z_x z}{-2z_x x - 2z_y y - z\alpha} \\ \tau &= \frac{2z_x z_y x - y(z_x^2 - z_y^2 + 1) - 2z_y z}{-2z_x x - 2z_y y - z\alpha} \end{aligned} \tag{22}$$

In [21], we show that $\Delta \geq 0$ and $\Delta = 0$ if and only if

$$\begin{aligned} z_{xx}(x^2 + z^2) - z_{yy}(y^2 + z^2) &= 0 \\ z_{xy} &= \frac{-xy(z_{xx}x^2 + z_{yy}y^2 + z^2(z_{xx} + z_{yy}))}{2(x^2 + z^2)(y^2 + z^2)} \end{aligned} \tag{23}$$

$A = 0$ and $B = 0$ if and only if

$$\begin{aligned} z_{xx} &= -\frac{y^2 + z^2}{2z(x^2 + y^2 + z^2)}, z_{xy} = \frac{xy}{2z(x^2 + y^2 + z^2)} \\ z_{yy} &= -\frac{x^2 + z^2}{2z(x^2 + y^2 + z^2)} \end{aligned} \tag{24}$$

In [21], we show that if $\Delta = 0$, the edge-parallel equations are zero, i.e., it is always a pinhole camera. Similarly, if $A = 0$ and $B = 0$, the edge parallel equations are also satisfied, i.e., there is no twisted orthographic cameras. Unlike the orthographic case when we choose a fixed 2PP, here we change the parametrization plane with the normal of the mirror surface. Thus, recovering the surface requires inverse Legendre transformation and is outside the scope of this paper.

In general, all reflections observed by a pinhole or an orthographic camera can be characterized as four types of GLCs: cross-slit, pushbroom, pinhole, or orthographic. No pencil, twisted orthographic, or bilinear cameras are observed. This is because these three cameras contain pure twisting rays [20] which cannot occur due to the fundamental geometric properties of the surface. In the future, we intend to further investigate the underlying theory.

6. Caustic Surfaces and GLCs

To show the relationship of the multiperspective GLC model to the caustic surface, we first compute the caustic surface using the Jacobian method [5, 17]. Consider each reflected ray is parameterized as (σ, τ, u, v) with source $S(u, v, 0)$ and direction $V(\sigma, \tau, 1)$. The Jacobian matrix $det[J(S + \lambda V)]$ can be computed as:

$$\begin{vmatrix} u_x + \lambda\sigma_x & v_x + \lambda\tau_x & \sigma \\ u_y + \lambda\sigma_y & v_y + \lambda\tau_y & \tau \\ 0 & 0 & 1 \end{vmatrix} = 0 \tag{25}$$

which corresponds to the same quadratic characteristic equation of the local GLC model as equation (8). Therefore, the unions of the solutions to the characteristic equation for every local GLC form the caustic surface. And because the roots of the characteristic equation often correspond to cross-slit cameras and have two solutions, caustics surfaces are formed in pairs. A similar result is shown in [18]. For rotationally symmetric mirrors viewed along its rotation axis, the rotation axis is one of the caustics.

The characteristic equation not only gives two caustic points, but also two slits, i.e., points with directions. In the conventional method, the caustic surface is regarded as the loci of the virtual viewpoint for every single ray. Our approach models the group behavior of nearby rays as a local GLC where rays simultaneously pass through the two slits, one on each of the caustic surfaces. Therefore, the obtained slits not only provide the caustic surface but also reveal a ruling upon it. In Figure 5, we illustrate three commonly used mirrors. The mirror surface is drawn in cyan, the caustic surface in blue and viewpoint as blue circle. Notice, the rotation axis is the second caustic surface for both hyperbolic and spherical mirrors. The slits are shown on the cyan

caustic surface as blue line segments. These rulings determine which rays lie on the local tangent GLC and the local distortions seen in the reflection, as we show in Section 7.

In addition, the spatial separation of the corresponding slits are also important. If the two slits intersect, the local GLC corresponds to a pinhole camera. Notice, the center of the hyperbolic and parabolic mirrors satisfy this condition, therefore the center of the image looks least distorted. In the cylindrical mirror, however, the two slits at the cusp do not intersect, which results in the apparent bending seen at the center of the image in Figure 6c.

The ruling of the slits on the caustic surface is closely related to the fact that the 3D caustic surface exists only if the reflected rays form a developable surface which is not a generalized cylinder or a cone [4, 13]. We intend to further investigate their relationship in the future.

7. Characteristic GLC Distortions

Our analysis has shown that reflections viewed from a pinhole or an orthographic camera off any mirror surface can only locally behave as one of the four GLC cameras. The reflection distortions seen in the reflected image can be completely characterized by analyzing the imaging property of these camera types.

7.1. Cross-slit Distortion

The image distortion of a cross-slit camera depends on the spatial relationship between the two slits and the image plane [22]. Specifically, if one slit is much closer to the image plane than the other, the orientation of the image will be dominated by the closer slit. In Figure 6, we compare the ray-traced reflection images seen from hyperbolic, parabolic and cylindrical mirrors. The ruling of the closer caustic surface, as shown in Figure 5, determines the orientation in the reflected image (e.g., the slit of the hyperbolic and parabolic mirrors form concentric circular patterns and the cylinder mirror exhibits bending vertical patterns, which can be observed in the reflections seen in Figure 6).

The distance between the two slits determines the aspect ratio distortions. Pushbroom, orthographic, and pinhole cameras can all be characterized as special cases of cross-slit cameras [22, 20]. When the two slits intersect, it transforms into a pinhole camera with small aspect ratio distortion. When one of the slits goes to infinity, the cross-slit transforms into a pushbroom camera with large aspect ratio distortions. In Figure 6, we plot the slit-distance image of the three mirrors. The hyperbolic mirror has an overall small distance map (6d), thus, its image (6a) has an uniform aspect ratio distortion. The spherical mirror has small distance map near the center, that grows larger near the boundary (6e). Thus, we observe more severe distortions near the boundary of the mirror than at the center (6b). The cylindrical mirror has an overall large distance map (6f), and the whole image (6c) is stretched vertically since the vertical slit is closer to the image plane.

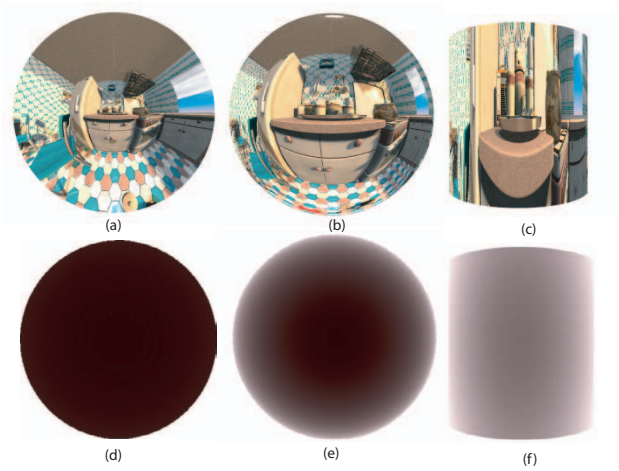

Figure 6. Aspect ratio distortion. Top row: reflected images of a hyperbolic, spherical, and cylinder mirror. Bottom row: estimated ratio distortion by the slits distance of the respective mirrors.

With one slit at infinity, the local GLC corresponds to a pushbroom, and things faraway will map to duplicate images, as shown in Figure 1c and 7c. Duplications often happen at the parabolic points when viewed from faraway, as we have shown in Section 4 for the orthographic camera case. A similar analysis is shown by Koenderink [10] for specular reflections.

7.2. Predicting Distortions on Mesh Surfaces

Reflections seen on a mesh surface are difficult to analyze using conventional methods. We can use a similar technique to that used to analyze a parametric surface. For each triangle of the mesh, we compute the three reflected rays from the vertexes and model it as a GLC. To minimize errors, we choose the average reflected direction of the rays as the normal direction of the parametrization plane. By computing the characteristic equation and two slits of the GLC for each triangle, we can measure their distances and estimate their aspect ratio and duplication distortions.

In Figure 7, we give an example of the pear-shaped mirror modelled by the following function

$$z = exp(-\frac{x^2+y^2}{0.15}) - (x^2+y^2) \qquad (26)$$

We discretize the surface as a triangle mesh, shown in Figure 7a. At each triangle, we compute the local GLC and show the distance map between the two slits in Figure 7b.

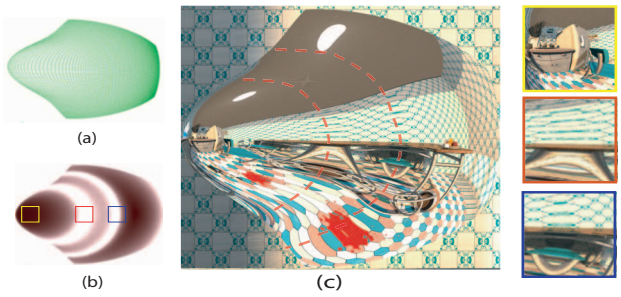

Figure 7. (a) A pear-shaped mesh. (b) Estimated distortions. Bright colors correspond to large distortions and dark colors correspond to small distortions. (c) A ray-traced image of the parametric surface.

The brightest region predicts where the pushbroom distortions occur. Figure 7(c) shows a ray traced image of the parametric surface. Our method predicts the low and high distortions regions, as shown in the yellow, red, and blue rectangle. In fact, the two bright bends estimated from the mesh surface correspond to the parabolic curve (red-dashed curve) of the surface. Duplicated reflections can be seen on either side of these parabolic curves, shown in the red and blue outlined regions.

8. Conclusions

We have presented a novel method for analyzing reflections on arbitrary surfaces using multiperspective cameras. We provide an analytical framework to locally model reflections as specific multiperspective cameras around every ray based on the theory of general linear cameras. Our framework better characterizes image distortions seen on irregular mirror surfaces as well as the conventional catadioptric mirrors. The local multiperspective model also reveals the relationship between the two caustic surfaces and reveals an important surface ruling of the caustics. Finally, our analysis provides useful information to design special featured mirrors or to avoid undesirable imagery properties.

References

[1] S. Baker and S. K. Nayar, "A Theory of Single-Viewpoint Catadioptric Image Formation," *International Journal on Computer Vision*, 35(2):1-22, 1999.

[2] C. Bellver-Cebreros and M. Rodraguez-DAnta, "Caustics and the Legendre Transformation," *Optics Communications*, 92(4-6):187–192, 1992.

[3] M. Born and E. Wolf, "Principles of Optics," *Permagon Press*, 1965.

[4] J. Bruce and P. J. Giblin, and C. G. Gibson, "Curves and Singularities," *Cambridge University Press*, second edition, 1992.

[5] D. G. Burkhard and D. L. Shealy, "Flux Density for Ray Propagation in Geometrical Optics," *Journal of the Optical Society of America*, 63(3):299–304, March 1973.

[6] J.Chahl and M. Srinivasan, "Reflective Surfaces for Panaromic Imaging," *Applied Optics*, 36(31):8275-8285, 1997.

[7] S. Gortler, R. Grzeszczuk, R. Szeliski, and M. Cohen, "The Lumigraph," *Proc. ACM SIGGRAPH '96 (1996)*, pp. 43–54.

[8] R. Gupta and R.I. Hartley, "Linear Pushbroom Cameras," *IEEE Trans. Pattern Analysis and Machine Intelligence*, vol. 19, no. 9 (1997) 963–975.

[9] S. B. Kang, "Catadioptric Self-calibration," In *Proc. CVPR*, I:201–207, June 2000.

[10] J. J. Koenderink, "Solid Shape," MIT Press, 1990.

[11] M. Levoy and P. Hanrahan,"Light Field Rendering," *Proc. ACM SIGGRAPH '96 (1996)*, 31–42.

[12] S. K. Nayar, "Catadioptric Omnidirectional Cameras," In *Proc. CVPR*, pages 482–488, 1997.

[13] M. Oren and S. K. Nayar, "A Theory of Specular Surface Geometry," *Int. Journal on Compute Vision*, 24:105–124, 1996.

[14] T. Pajdla, "Stereo with Oblique Cameras," *Int'l J. Computer Vision*, vol. 47, nos. 1/2/3 (2002) 161–170.

[15] W. Stürzl, H. J. Dahmen, and H. Mallot, "The Quality of Catadioptric Imaging–Application to Omindirectioinal Stereo," *Proc. 8th European. Conf. on Computer Vision (ECCV 2004)*, 614-627.

[16] R. Swaminathan and S. K. Nayar, "A Perspective on Distortions," In *Proc. IEEE Computer Vision and Pattern Recognition (CVPR)*, Wisconsin, June 2003.

[17] Rahul Swaminathan, Michael D. Grossberg, and Shree K. Nayar, "Caustics of Catadioptric Cameras," *Proc. of IEEE International Conference on Computer Vision*, Vancouver, Canada, July 2001.

[18] R. Swaminathan, M. D. Grossberg, and S. K. Nayar, "Non-Single Viewpoint Catadioptric Cameras: Geometry and Analysis," *Technical Report CUCS-004-01*, Dept. of Computer Science, Columbia University, 2001.

[19] Y. Yagi, S. Kawato, and S. Tsuji, "Real-time Omnidirectional Image Sensor (copis) for Vision-Guided Navigation," *Robotics and Automation*, 10(1):11–22, February 1994.

[20] J. Yu and L. McMillan, "General Linear Cameras," *Proc. 8th European. Conf. on Computer Vision (ECCV 2004)*, Volume II 14-27.

[21] J. Yu and L. McMillan, "Ray Geometry under Two Plane Parametrization," *MIT CSAIL Technical Report*, to appear.

[22] A. Zomet, D. Feldman, S. Peleg, and D. Weinshall, "Mosaicing New Views: The Crossed-Slits Projection," *IEEE Trans. on PAMI (2003)* 741–754.